Tuning Surface Spin Polarization of CoFeB by Boron Diffusion Detected by Spin Resolved Photoemission

Qi Liu[1†], Xianyang Lu[1,4†*], Chengrui Fu[2], Jiarui Chen[3], Zhe Zhang[1], Yuting Gong[1], Xinyue Wang[1], Yu Yan[1,4], Qinwu Gao[1], Hui Li[2*], Xuezhong Ruan[1], Yao Li[1], Jun Du[3], Jing Wu[4], Liang He[1], Bo Liu[5], Rong Zhang[1], and Yongbing Xu[1,4*]

[1]*Jiangsu Provincial Key Laboratory of Advanced Photonic and Electronic Materials, School of Electronic Science and Engineering, Nanjing University, Nanjing 210093, China*
[2]*Key Laboratory for Liquid-Solid Structural Evolution and Processing of Materials (Ministry of Education), Shandong University, Jinan 250061, China*
[3]*Department of Physics, Nanjing University, Nanjing 210093, China*
[4]*York-Nanjing Joint Center (YNJC) for Spintronics and Nano-engineering, Department of Electronics and Physics, University of York, York YO10 5DD, UK*
[5]*Key Laboratory of Spintronics Materials, Devices and Systems of Zhejiang Province, Hangzhou 311300, China*

(Received 6 May 2023; accepted manuscript online 12 July 2023)

Research of spin polarization of magnetic CoFeB thin films is of practical importance in spintronic applications. Here, using a direct characterization technique of spin-resolved photoemission spectroscopy, we obtain the surface spin polarization of amorphous $Co_{40}Fe_{40}B_{20}$ thin films with different annealing temperatures from 100 ℃ to 500 ℃ prepared by magnetron sputtering. After high annealing temperature, a quasi-semiconductor state is gradually formed at the CoFeB surface due to the boron diffusion. While the global magnetization remains almost constant, the secondary electrons' spin polarization, average valence band spin polarization and the spin polarization at Fermi level from spin-resolved photoemission spectroscopy show a general trend of decreasing with the increasing annealing temperature above 100 ℃. These distinct surface properties are attributed to the enhanced Fe–B bonding due to the boron segregation upon surface after annealing as confirmed by x-ray photoelectron spectroscopy and scanning transmission electron microscopy with energy dispersive spectroscopy. Our findings provide insight into the surface spin-resolved electronic structure of the CoFeB thin films, which should be important for development of high-performance magnetic random-access memories.

DOI: 10.1088/0256-307X/40/8/087302

CoFeB-based magnetic tunnel junctions (MTJs) are a kind of the most studied spintronic devices due to their high tunneling magnetoresistance (TMR) and low switching current density. The TMR ratio is fundamentally determined by the spin polarization P owing to Jullière's formula $\mathrm{TMR} = (2P_1P_2)/(1-P_1P_2)$, where P_1 and P_2 represent the spin polarizations of each ferromagnetic electrode in MTJs, respectively.[1] High TMR ratio is the key for MTJ based magnetic random-access memories (MRAMs) requiring a large switch ratio, which is dependent on the spin polarization. Furthermore, the spin polarization is also a key parameter for spin transfer torque switching and the critical current density is important for current-driven domain wall motion.[2,3] Spin polarization P of CoFeB, defined as a normalized difference of the density of states (DOS) between spin-up and spin-down electrons at Fermi level E_F, has been experimentally measured by several methods under different growth conditions. The spin polarization was estimated to be 51% in the $CoFeB/Al_2O_3/CoFeB$ MTJ with a TMR value of 70%, simply according to Jullière's formula.[4] However, when the TMR value was demonstrated to be up to 604% in CoFeB/MgO/CoFeB MTJ at room temperature, the limitation of Jullière's model emerges and the spin polarization is not accessible in this way.[5–7] It was found that the tunneling spin polarization (TSP) is significantly enhanced from 0.22 for CoFeB-AlO_x based MTJs to 0.46 for CoFeB-MgO based MTJs by analyzing the critical current in spin transfer switching process.[8] Recently, a quite low spin polarization down to 0.26 was obtained by moving domain walls in Ta/CoFeB/MgO nanowires, which may be influenced by the heavy-metal Ta layer.[9] Using point-contact Andreev reflection technique, spin polarization of as much as 65% is achieved and it is found that the crystallization of the amorphous state reduces the spin polarization after annealing.[10] Furthermore, a series of studies used the superconducting tunneling spectroscopy technique to obtain the TSP of amorphous CoFeB.[11–14] The measured TSP value of 53% was shown to be in good agreement with the calculated s-electron spin polarization, supporting the proposed theory that s-like electrons have the highest transmittance in the MTJs with fourfold symmetric crystalline structures. However, all the mentioned methods to achieve the (tunneling) spin polarization of CoFeB are not in a direct way, which means that the values are obtained by fitting the other measured physical quantities. Meanwhile,

†Q. Liu and X. Lu contributed equally to this work.
*Corresponding authors. Email: xylu@nju.edu.cn; lihuilmy@sdu.edu.cn; ybxu@nju.edu.cn
© 2023 Chinese Physical Society and IOP Publishing Ltd

it is well known that the interface properties play a critical role for performance of MTJs, for example, the perpendicular magnetic anisotropy in MTJs has been attributed to the change of the local atom bonding or lattice constant at the interface.[15] The suitable stoichiometry and roughness at the interface were also proposed to enhance the TMR value.[16] Hence, the spin polarization of the interface or surface of amorphous CoFeB is crucial and has not been conclusively determined.

In this Letter, we report our direct observation of spin polarization of CoFeB thin films grown by magnetron sputtering using spin-resolved photoemission spectroscopy. As the post-annealing process is key to improve the interface properties and then to achieve large TMR, we systematically study CoFeB films with different annealing temperatures. The x-ray photoelectron spectroscopy (XPS) and scanning transmission electron microscopy with energy dispersive spectroscopy (STEM-EDS) measurements indicate that the boron atoms tend to diffuse towards the top surface of the CoFeB layer after annealing, causing a quasi-semiconductor state on the surface. Furthermore, we find that the electronic structure in the surface of CoFeB is mainly dominated by Fe–B bonding interaction, which is significantly associated with the diffused boron atoms at the sample surface. The annealing temperature dependence of the secondary electrons' spin polarization, average valence band spin polarization and the spin polarization at Fermi level are all distinctively different from those of the global saturation magnetization obtained with a vibrating sample magnetometer.

Experimental Details. The sample structure in this work is shown in Fig. 1(a). A 10-nm-thick $Co_{40}Fe_{40}B_{20}$ thin film was deposited onto a thermally oxidized Si(100) substrate with a 10 nm Ta underlayer at ambient temperature using direct current magnetron sputtering with a base pressure below 10^{-8} Torr. The sputtering rates for Ta and CoFeB were about 0.22 Å/s and 0.12 Å/s, respectively, while the working argon pressure was 5×10^{-3} Torr. The samples were *in situ* post-annealed at different temperatures (T_a = 100, 200, 300, 400, 500 ℃) for 30 min and then magnetized by applying an in-plane magnetic field of about 500 Oe in the same chamber. Since the coercive fields of all samples are less than 250 Oe, the applied magnetic field is high enough to saturate the films. Then, the CoFeB thin film was kept at magnetic remanence for the later photoemission spectrum measurement. The spin-resolved and angle-resolved photoemission spectroscopy (ARPES) setup is schematically illustrated in Fig. 1(b), which consists of an unpolarized helium lamp (Fermi BL1010s VUV) with the photon energy of 21.2 eV and an SPECS PHOIBOS 150 hemisphere energy analyzer equipped with a 3D micro-Mott detector operated at a scattering energy of 25 kV. Four channels in the Mott detector were used to measure both in-plane and out-of-plane spin components. The energy resolution is 160 meV and the effective Sherman function S_{eff} is 0.16.[17] The base pressure of the vacuum chamber was better than 10^{-10} Torr for spin-resolved photoemission experiments. It is worth noting that the chambers for sample preparation and spin-resolved photoemission measurement were connected via an ultrahigh vacuum tube with a base pressure better than 10^{-10} Torr to avoid surface contaminations. The magnetic hysteresis loops were measured using a vibrating sample magnetometer (VSM), the elemental analysis and the elemental spatial distribution were characterized by XPS and STEM-EDS, respectively. These films were capped with a 3 nm MgO layer for *ex situ* measurements before transferred from the ultrahigh vacuum chamber. All the experiments were performed at room temperature.

Results and Discussions. The magnetic hysteresis loops of the CoFeB films with different annealing temperatures are shown in Fig. 1(c). The as-deposited CoFeB film is magnetically soft with a small coercive field (∼7 Oe). While the saturate magnetization remains stable, the coercive field as a function of the annealing temperature (see Fig. S2 in the Supplementary Material) shows a drastic increase when the annealing temperature is above 300 ℃. This observation is in good agreement with the previous results, which is attributed to the partial crystallization of the originally amorphous films.[10,18] In this case the local crystalline FeCo structure is formed via the diffusion of the boron atoms towards the interfaces.

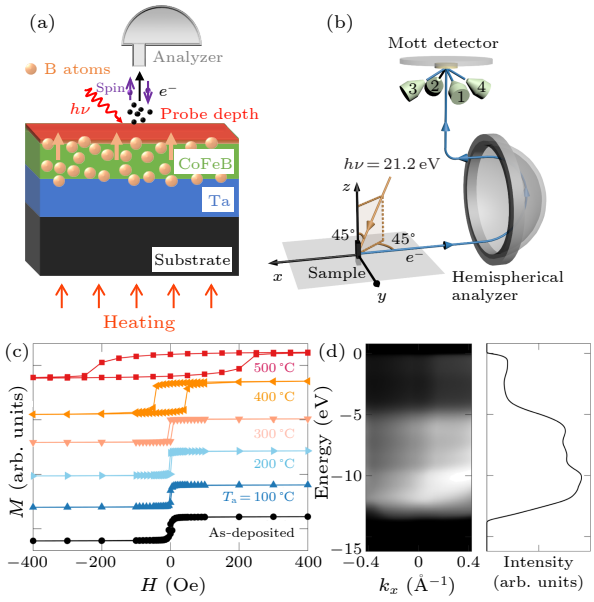

Fig. 1. (a) Schematic illustration of the sample structure. The orange and purple arrows represent the diffusion tendency for B atoms and the up- and down-spins of the photoelectrons, respectively. (b) Instruction diagram of the spin-resolved photoemission system. (c) In-plane magnetization hysteresis loops at room temperature of the as-deposited and annealed films. (d) The spectrum for ARPES measurement (left panel) and the corresponding EDC (right panel) of the as-deposited CoFeB thin film.

The spectrum of ARPES measurement of the as-deposited CoFeB thin film is shown in Fig. 1(d). It shows that there is no clear band dispersion since the sample is amorphous. The angular-integrated energy distribution curve (EDC) is presented in the right panel. ARPES spectra of amorphous CoFeB at different annealing temperatures could be found in section S1 of the Supplementary Material. Figure 2(a) shows the EDCs obtained by spin-integrated photoemission spectra of the as-deposited and annealed films. For the as-deposited CoFeB film (shown

by the black line), the measured EDC exhibits two broad peaks around E_F and 5.5 eV below E_F, which are from 3*d* electronic states of transition metals and 2*p* electronic states of boron, respectively.[19] With increasing annealing temperature, the intensity of 3*d* peak (transition metal) decreases while the intensity of 2*p* peak (boron) increases upon annealing. For intuitive comparison, the intensity ratio between 2*p* peak originated from boron and 3*d* peak originated from Fe and Co are summarized in the inset of Fig. 2(a). Considering that the escape depth of photoelectrons is about 6 Å with the photon energy of 21.2 eV in our experimental setup [shown by the red area in Fig. 1(a)], the increasing intensity ratio with rising annealing temperature indicates that the sample surface is gradually dominated by the boron atoms.[20,21] Surprisingly, almost no electrons are probed around E_F when the annealing temperature reaches 500 ℃, implying that the quasi-semiconductor state is formed at the CoFeB surface.

Then, XPS is conducted to verify the elements' evolution with annealing temperature in the CoFeB layer. Before the *ex situ* XPS measurements, Ar^+ ion sputtering with a rate about 0.4 nm/min was performed for 20 min so that the measured spectra reflect the elemental composition mostly from the bulk rather than the surface of the CoFeB films, as demonstrated in section S4 of the Supplementary Material. As shown in Figs. 2(b)–2(c), by comparing the as-deposited and the annealed film, the intensity of the B 1*s* peak decreases while the intensities of the Co, Fe 2*p* peaks increase for the annealed sample. This means that the content of B decreases in the bulk material. By assuming that the element's content in total is stable in the structure, the variation for each element with annealing temperature in the bulk material is expected to exhibit the tendency opposite to that on surface. Thus, the decrease boron content in bulk suggests that boron atoms diffuse towards surface after annealing.

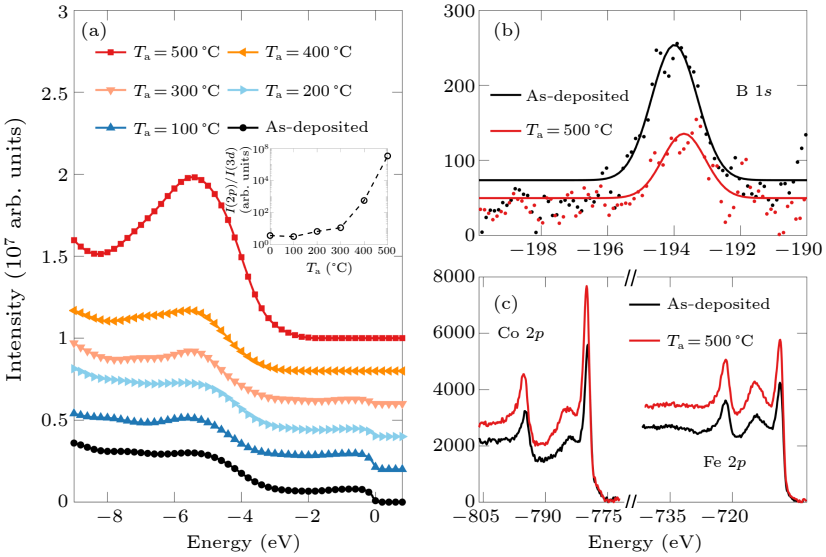

Fig. 2. (a) Spin-integrated photoemission spectra of the CoFeB thin film. The intensity ratio between 2*p* peak and 3*d* peak with increasing annealing temperature is summarized in the inset. [(b), (c)] XPS spectra of the as-deposited and the film annealed at 500 ℃, as shown in the black and red line, respectively. The lines in (b) are Gaussian fits of raw data (dots) to guide to eyes.

To further investigate the composition of the CoFeB films, especially the B atoms distribution, STEM-EDS is used to directly observe the elemental distribution. The cross-section view and the EDS maps are presented in the Supplementary Material. For both as-deposited and annealed cases, as shown in Fig. S6, a significant portion of B has extended into the Ta underlayer, while Co and Fe atoms can maintain the stoichiometric proportion with excellent stability. There are, however, distinct differences in respect of distribution and content of B atoms, as the line profiles shown in Figs. S7(c) and S7(d). On the one hand, considering the downwards edge of diffused B atoms, the annealed sample possesses a shallower diffusion length in the Ta layer. On the other hand, the global B content reduces after annealing. More detailed analysis is included in section S5 of the Supplementary Material. These variations indicate that the boron atoms diffuse upwards (towards the CoFeB top surface) after annealing, which is consistent with the deduction using photoemission and XPS measurements.

We now focus on the spin polarization measured by spin-resolved photoemission spectroscopy (SRPES). To avoid any error introduced into the measurement by apparatus asymmetries, two measurements of the spin polarization were necessarily made, one with the sample magnetized 'up' ($I_L^+ I_R^+$) and the other with the sample magnetized 'down' ($I_L^- I_R^-$). Here I_L and I_R represent the number of electrons scattered from the target into the left and right channels, respectively. The spin polarization P is calculated by[22]

$$P = \frac{1}{S_{\text{eff}}} \frac{\sqrt{I_L^+ I_R^-} - \sqrt{I_L^- I_R^+}}{\sqrt{I_L^+ I_R^-} + \sqrt{I_L^- I_R^+}}. \quad (1)$$

As shown in Fig. 3, the measured spin polarization profiles of the amorphous CoFeB are consistent with the results of transition metal-boron alloys.[23] For samples annealed at lower temperatures ($T_a < 500$ ℃), spin polarizations

are negative at E_F [the green line in Figs. 3(a)–3(f)]. A broad peak at around −3 eV and a shallow minimum at about −5 eV are shown. As demonstrated in $Fe_{75}B_{25}$ and $Co_{77}B_{23}$, the former is mainly caused by the net negative spin polarization of B 2*p* states hybridized with Fe 3*d* states, whereas the latter corresponds to emission of electrons due to B 2*p*-derived states.[23,24] The spin polarization at E_F as a function of the annealing temperature is shown in Fig. 3(g). The negative spin polarization of −15% for the as-deposited CoFeB film increases to around −25% compared to the film annealed at 100 ℃. The value of the spin polarization decreases to smaller negative values with further increase of T_a. We note that when the annealing temperature reaches 500 ℃, the quasi-semiconductor surface state makes the spin polarization measured at Fermi level [Fig. 3(f)] meaningless since barely no counts are detected at E_F.

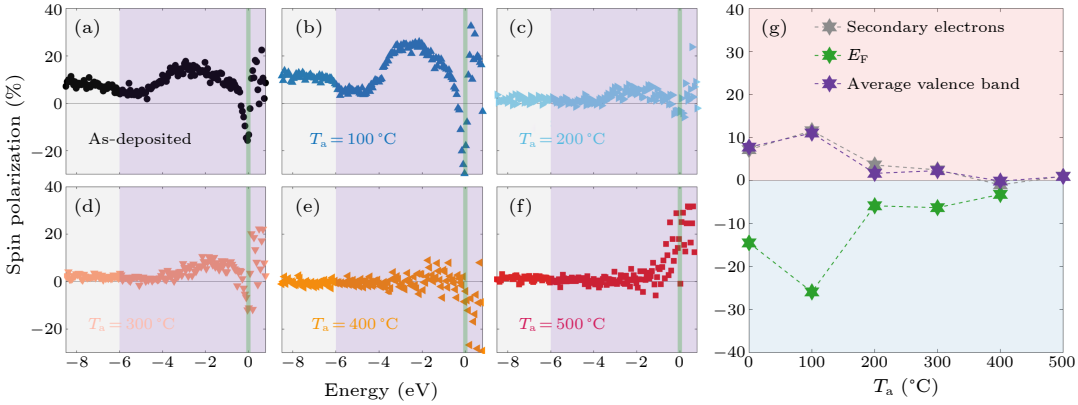

Fig. 3. (a)–(f) Spin polarizations of as-deposited and annealed CoFeB films. The grey and purple areas represent the energy ranges where the signals are dominated by secondary electrons and valence electrons, respectively. The green line shows the Fermi level. (g) Secondary electron and average valence band polarizations versus annealing temperature, as indicated by grey and purple stars, respectively. Spin polarization at Fermi level is represented by green stars.

We define that the energy region from −6 eV to the Fermi level is dominated by the valence electrons [purple areas in Figs. 3(a)–3(f)] while the secondary electrons mainly contribute to the energy region below −6 eV [gray areas in Figs. 3(a)–3(f)]. For the as-deposited sample and the annealed CoFeB film at 100 ℃, the spin polarization of the secondary electrons exhibits a slightly upshift with decreasing binding energy. This upshift feature is attributed to the 3*d* ferromagnets in surface region.[25] With higher annealing temperatures, the curves in this area are flattened, implying a weaker ferromagnetism. Meanwhile, the flatten region, which reflects the magnetism of the surface, approaches nearly zero after higher annealing temperature.[25] This is due to the fact that surface is gradually dominated by non-magnetic boron atoms with increasing annealing temperature. The values of the spin polarization at −8.5 eV, corresponding to the secondary electron polarizations of CoFeB thin films, are displayed in Fig. 3(g). It is shown that the secondary electrons' spin polarization initially increases and then decreases with higher annealing temperature.

The spin-resolved EDCs of CoFeB films annealed at different temperatures are shown in Fig. 4, where we distinguish the electronic structures for both spin channels. For all the samples, there are both spin states detected at Fermi level, showing no evidence of strong ferromagnetism. With the higher annealing temperatures, the separation between the majority-spin states and the minority-spin states becomes much smaller, implying a reduced effective exchange splitting. To understand the experimentally measured spin-resolved EDCs, first-principle calculations are performed within density functional theory using the Vienna *ab initio* simulation package.[26,27] The calculation details can be found in the Supplementary Material. The theoretical spin-resolved DOS each shows double peaks near E_F together with a low-intensity shoulder-like peak around −5.5 eV. Compared to the theoretical results, the much stronger peak around −5.5 eV experimentally measured is closely related to the cross section and the probing depth depending on the electron kinetic energy.[28] Contrary to our experimental results, the minority states clearly dominate around E_F with an effective exchange splitting of ∼2 eV theoretically. Bases on ligand field theory, the disagreement between the spin-resolved experimental and theoretical EDC's is essentially a discrepancy in the bonding and antibonding band splitting. This is closely related to the local structure of the amorphous state, as proposed in FeY before.[29,30] Specifically, the discrepancy may be arisen because the model structures for amorphous materials are idealized and homogenous in theoretical simulations, and these will certainly differ to some extent from the experimental bulk structure. Moreover, the theoretical DOS is bulk-like and may not be a suitable case for the surface and near-surface regions, which mainly contribute to the probed electronic structures by the electron spectroscopic techniques here. This gives us a hint that the electron structure of the surface state differs from that of the bulk state in CoFeB, which demonstrates the necessity of the direct measurements of surface spin polarization here. In addition, the averaged polarization of the valence band photoemission calculated from spin-resolved EDCs is shown in Fig. 3(g).

The averaged polarization is about 8% for the as-deposited CoFeB film and increases to 11% for the sample annealed at 100 ℃. Then it drops to nearly zero with increasing annealing temperature. This T_a dependence is coincident with the spin polarization of the secondary electrons as shown in Fig. 3(g). We note that the polarization of the secondary electrons is significantly higher than that of the averaged valence band, which is expected for transition metals or alloys.[25,29,31]

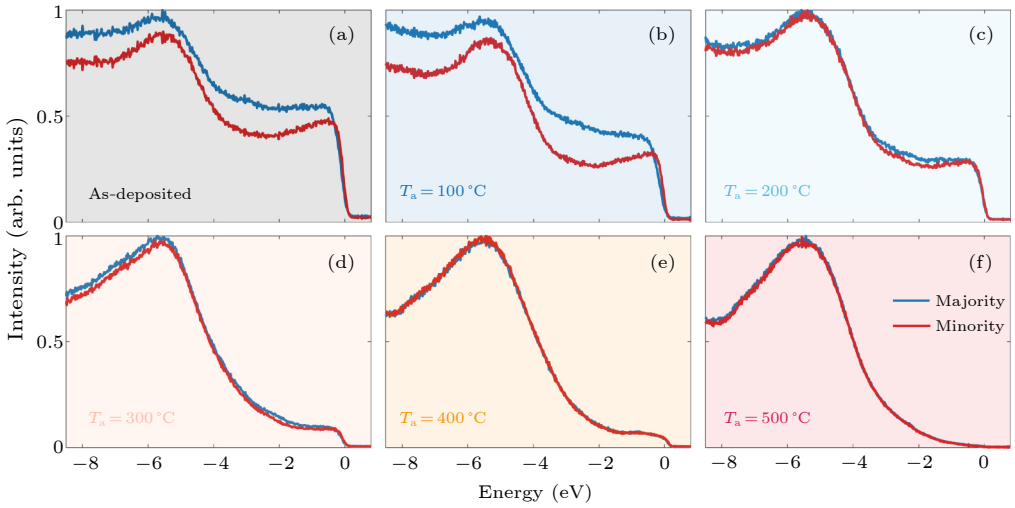

Fig. 4. Spin-resolved EDCs of CoFeB films at different annealing temperatures.

Overall, the spin polarization at Fermi level, the spin polarization of secondary electrons and the averaged spin polarization of valence band show a consistent trend as a function of annealing temperature. It firstly increases and subsequently decreases with increasing annealing temperature. As the boron atoms are likely to diffuse to surface by post annealing and the photoemission spectroscopy only probes the topmost layers, we can simply consider the effect of the composition at film surface. Amorphous CoB and FeB alloys have been theoretically studied.[32,33] In terms of amorphous Co–B alloys, because of the enhancement of the hybridization between the Co 3*d* states and the B 2*p* states, the exchange splitting of Co 3*d* states decreases with increasing B content. As a result, the ferromagnetism of amorphous Co–B alloys, as well as its spin polarization, becomes weaker as their B content increases.[32] The situation is more complicated in Fe–B alloy cases, where the magnetic moment increases at first and then decrease with increasing B content. The enhancement of the moment for lower B content arises from the competition between ferromagnetic and antiferromagnetic exchange interactions. The decrease with higher B content is due to a dilution effect: polarizable *d*–*d* bonds are replaced by magnetically inert *p*–*d* bonds.[33] As our measured spin polarizations of CoFeB films with annealing temperature has a similar trend compared to the magnetization of FeB alloys with B content, it is inferred that B atoms are likely to bond with Fe atoms and the Fe–B bond dominates the surface spin polarization. This may associate with the higher content of Fe relative to that of Co in the surface region, since the relatively content of Fe in the bulk reduces after annealing compared to that of Co, as shown in Fig. 2(c) and demonstrated in section S7 of the Supplementary Material. Additionally, the magnetic moments and the tunnelling spin polarization of $Co_{1-x}Fe_x$ alloy display the Slater–Pauling behavior, which is the well-known deviation from a linear change. A maximum of the tunneling spin polarization is shown as the alloy composition changes in $Co_{1-x}Fe_x$, which is consistent with the tendency of spin polarization observed in this work.[14]

It is worthy to mention that the influence of oxygen absorption on the film surface can be excluded in our measurement. Firstly, all the annealed samples are transferred to the SRPES chamber via an ultrahigh vacuum tube as soon as possible. In this case the intensity of the oxygen absorption, if it indeed exists, would be similar for all the samples. Secondly, it is reported that the spin polarization in the regime of the metallic 3*d* emission remains essentially unchanged with oxygen adsorption, although the oxygen peak is clearly distinguished in the EDCs.[34] This means that the oxygen absorption on the surface would not alter the spin polarization of the sample itself. In our measurements, however, the quenched magnetism and spin polarization are clearly shown as annealing temperature increases. Therefore, the observed varied spin polarization is solely dependent on the annealing temperature.

In summary, we have experimentally obtained the surface spin polarization of sputtering-grown amorphous CoFeB thin films using spin-resolved photoemission. By analyzing the XPS and STEM-EDS results, it is found that with increasing annealing temperature, the boron atoms diffuse towards the top surface region and eventually resulting in a quasi-semiconductor state at the CoFeB surface. Furthermore, distinct from the stable global saturation magnetization obtained with a VSM, the secondary electrons' spin polarization, average valence band spin polarization and the spin polarization at Fermi level follow the same trend of decreasing as the annealing temperature rises above 100 ℃. In the surface of CoFeB thin films, the electronic state is ascribed to be mainly dom-

inated by variation in Fe–B bonding interaction. The combination of *in situ* sputtering and spin-resolved electron spectroscopy measurements provides excellent platform for a broad range of experimental investigation of the spin-dependent electronic structure of magnetic amorphous alloys. Furthermore, as the switch ratio of MTJ-based MRAM is determined by the interface spin polarization, our results demonstrate that the boron segregation may be a key factor to influence the performance of MRAM.

Supplementary Material. The Supplementary Material includes the spectra for ARPES measurements, coercive field and saturate magnetization versus the annealing temperature, the evolution of spin-integrated photoemission spectra around Fermi level, the experimental details in XPS measurements, the cross-section view of STEM images, EDS mappings and line profile, methods for calculating the spin polarization and spin-resolved spectra, the content ratio between Fe and Co from XPS, the calculated spin-resolved density of states for amorphous CoFeB.

Acknowledgements. This work was supported by the National Key Research and Development Program of China (Grant No. 2021YFB3601600), the National Natural Science Foundation of China (Grant Nos. 12104216, 61427812, 11774160, 51971109, 51871236, 51771053, and U1806219), the Natural Science Foundation of Jiangsu Province of China (Grant Nos. BK20200307, BK20192006, and BK20180056), and the Fundamental Research Funds for the Central Universities (Grant No. 21014380113).

References

[1] Julliere M 1975 *Phys. Lett. A* **54** 225
[2] Meng H, Sbiaa R, Lua S Y H, Wang C C, Akhtar M A K, Wong S K, Luo P, Carlberg C J P, and Ang K S A 2011 *J. Phys. D* **44** 405001
[3] Zhang W, Wong P K J, Zhou X, Rath A, Huang Z, Wang H, Morton S A, Yuan J, Zhang L, Chua R, Zeng S, Liu E, F X, A, Chua D H C, Feng Y P, van der Laan G, Pennycook S J, Zhai Y, and Wee A T S 2019 *ACS Nano* **13** 2253
[4] Wang D, Nordman C, Daughton J M, Qian Z, Fink J, Wang D, Nordman C, Daughton J M, Qian Z, and Fink J 2004 *IEEE Trans. Magn.* **40** 2269
[5] Djayaprawira D D, Tsunekawa K, Nagai M, Maehara H, Yamagata S, Watanabe N, Yuasa S, Suzuki Y, and Ando K 2005 *Appl. Phys. Lett.* **86** 092502
[6] Ikeda S, Hayakawa J, Ashizawa Y, Lee Y M, Miura K, Hasegawa H, Tsunoda M, Matsukura F, and Ohno H 2008 *Appl. Phys. Lett.* **93** 082508
[7] MacLaren J M, Zhang X G, and Butler W H 1997 *Phys. Rev. B* **56** 11827
[8] Diao Z T, Apalkov D, Pakala M, Ding Y F, Panchula A, and Huai Y M 2005 *Appl. Phys. Lett.* **87** 232502
[9] Zhang X Y, Vernier N, Vila L, Yan S H, Cao Z Q, Cao A N, Wang Z L, Cai W L, Liu Y, Yang H W, Ravelosona D, and Zhao W S 2019 *Phys. Rev. Appl.* **11** 054041
[10] Huang S X, Chen T Y, and Chien C L 2008 *Appl. Phys. Lett.* **92** 242509
[11] Paluskar P V, Kohlhepp J T, Swagten H J M, and Koopmans B 2006 *J. Appl. Phys.* **99** 08e503
[12] Paluskar P V, Kohlhepp J T, Swagten H J M, Koopmans B, Wolters R, Boeve H, and Snoeck E 2007 *J. Phys. D* **40** 1234
[13] Swagten H J M, Paluskar P V, Lavrijsen R, Kohlhepp J T, and Koopmans B 2007 *J. Magn. Magn. Mater.* **310** 2012
[14] Paluskar P V, Lavrijsen R, Sicot M, Kohlhepp J T, Swagten H J, and Koopmans B 2009 *Phys. Rev. Lett.* **102** 016602
[15] Li Z P, S L, Zheng Y, Fang J, Chen L, Hong L, and Wang H 2016 *Appl. Phys. Lett.* **109** 182403
[16] Lou Y, Zhang Y, Guo H, Xu D, and Zhang Y 2017 *J. Semicond.* **38** 062003
[17] Zhang X, Xu H, Lai B, Lu Q, Lu X, Chen Y, Niu W, Gu C, Liu W, Wang X, Liu C, Nie Y, He L, and Xu Y 2018 *Sci. Rep.* **8** 8074
[18] Cardoso S, Cavaco C, Ferreira R, Pereira L, Rickart M, Freitas P P, Franco N, Gouveia J, and Barradas N P 2005 *J. Appl. Phys.* **97** 10C916
[19] Hopster H, Kurzawa R, Raue R, Schmitt W, Guntherodt G, Walker K H, and Guntherodt H J 1985 *J. Phys. F* **15** L11
[20] Seah M P and Dench W A 1979 *Surf. Interface Anal.* **1** 2
[21] Zhang Z, Lu X, Yan Y, Lu J, Li Z, Liu Q, Zhu F, Cao J, Wang Y, Huang Z, Zhai Y, Li Y, Ruan X, He L, Wu J, Du J, Zhang R, and Xu Y 2022 *Appl. Phys. Lett.* **120** 182403
[22] Seddon E A 2016 *Spin-Resolved Valence Photoemission.* In Xu Y, Awschalom D, and Nitta J (eds) *Handbook of Spintronics* (Berlin: Spinger) pp 831–918
[23] Xu Y B, Greig D, Seddon E A, Cornelius S, and Matthew J A D 1999 *IEEE Trans. Magn.* **35** 3427
[24] Xu Y B, Greig D, Seddon E A, and Matthew J A D 2000 *J. Appl. Phys.* **87** 7136
[25] Hopster H 1987 *Phys. Rev. B* **36** 2325
[26] Kresse G and Furthmuller J 1996 *Phys. Rev. B* **54** 11169
[27] Kresse G and Hafner J 1993 *Phys. Rev. B* **47** 558
[28] Yeh J J and Lindau I 1985 *At. Data Nucl. Data Tables* **32** 1
[29] Xu Y B, Greig D, Seddon E A, and Matthew J A D 1997 *Phys. Rev. B* **55** 11442
[30] Stöhr J and Siegmann H C 2006 *Springer Series in Solid-State Sciences* (Berlin: Springer) vol 152 p 216
[31] Penn D R, Apell S P, and Girvin S M 1985 *Phys. Rev. Lett.* **55** 518
[32] Tanaka H, Takayama S, Hasegawa M, Fukunaga T, Mizutani U, Fujita A, and Fukamichi K 1993 *Phys. Rev. B* **47** 2671
[33] Hafner J, Tegze M, and Becker C 1994 *Phys. Rev. B* **49** 285
[34] Schmitt W, Hopster H, and Guntherodt G 1985 *Phys. Rev. B* **31** 4035